Estuaries and Coasts Vol. 29, No. 1, p. 81–95 February 2006

Relative Effects of Physical and Biological Processes on Nutrient and Phytoplankton Dynamics in a Shallow Estuary After a Storm Event

STEPHANIE K. MOORE[1,*], MARK E. BAIRD[2], and IAIN M. SUTHERS[1]

[1] *Fisheries and Marine Environmental Research Laboratory, School of Biological, Earth and Environmental Sciences, University of New South Wales, Sydney, New South Wales 2052, Australia*
[2] *Centre for Environmental Modelling and Prediction, School of Mathematics, University of New South Wales, Sydney, New South Wales 2052, Australia*

ABSTRACT: The effects of advection, dispersion, and biological processes on nitrogen and phytoplankton dynamics after a storm event in December 2002 are investigated in an estuary located on the northern New South Wales coast, Australia. Salinity observations for 16 d after the storm are used to estimate hydrodynamic transports for a one-dimensional box model. A biological model with nitrogen limited phytoplankton growth, mussel grazing, and a phytoplankton mortality term is forced by the calculated transports. The model captured important aspects of the temporal and spatial dynamics of the bloom. A quantitative analysis of hydrodynamic and biological processes shows that increased phytoplankton biomass due to elevated nitrogen loads after the storm was not primarily regulated by advection or dispersion in spite of an increase in river flow from < 1 to 928×10^3 m^3 d^{-1}. Of the dissolved nitrogen that entered the surface layer of the estuary in the 16 d following the storm event, the model estimated that 28% was lost through exchange with the ocean or bottom layers, while 15% was removed by the grazing of just one mussel species, *Xenostrobus securis*, on phytoplankton, and 50% was lost through other biological phytoplankton loss processes. *X. securis* grazing remained an important loss process even when the estimated biological parameters in the model were varied by factors of $\pm$ 2. The intertidal mangrove pneumatophore habitat of *X. securis* allows filtering of the upper water column from the lateral boundaries when the water column is vertically stratified, exerting top-down control on phytoplankton biomass.

Introduction

The interaction between hydrodynamic processes and nutrient dynamics in controlling phytoplankton growth and accumulation in estuaries has been demonstrated on seasonal and annual time scales (Jassby et al. 1990; Mallin et al. 1993; Basu and Pick 1996; Robson and Hamilton 2003). The relative influence of these processes is highly dependent on rainfall, which can deliver large nutrient loads to estuaries and initiate phytoplankton blooms, especially for altered catchments and storm events (Hama and Handa 1994; Eyre and Pont 2003; Scharler and Baird 2003). Rainfall also influences estuarine hydrodynamic processes that can either prevent or contribute to the accumulation of phytoplankton biomass. Increased river flow after rainfall can decrease water residence times and prevent phytoplankton biomass accumulation (Cloern et al. 1985). The delivery of fresher water to estuaries after rainfall can also enhance vertical density gradients resulting in a stratified water column. Under these conditions vertical mixing is reduced and phytoplankton biomass can accumulate in the upper water column where conditions for growth are more favorable (Koseff et al. 1993). Few studies have examined these interactions over short (daily) time scales immediately following storms (see Eyre and Twigg 1997; Eyre 2000; Ferguson et al. 2004).

Biological processes such as grazing can also regulate phytoplankton accumulation in estuaries. Filter-feeding bivalve molluscs are effective grazers capable of removing phytoplankton at rapid rates from large volumes of water (Cloern 1982; Alpine and Cloern 1992; Caraco et al. 1997). *Dreissena polymorpha* has been found to filter a volume of water equivalent to the entire tidal freshwater portion of the Hudson River, New York, every 2 d (Roditi et al. 1996). In Saginaw Bay, Lake Huron, United States, the population of *D. polymorpha* can filter the entire water volume of the inner bay in 0.5 to 0.8 d (Bridgeman et al. 1995). In these systems, filter-feeding bivalves can exert top-down control on phytoplankton and act as biological buffers to the effects of nutrient enrichment, but storms can considerably hamper the ability of filter-feeding bivalves to regulate estuarine phytoplankton blooms.

* Corresponding author; current address: University of Washington, School of Oceanography, Box 355351, Seattle, Washington 98195-5351; tele: 206/543-0599; fax: 206/685-3354; e-mail: stephanie.moore@UNSWalumni.com

Large sudden changes in salinity after storms can reduce physiological activity and cause filter-feeding bivalves to close their shells. Depending on the extent of the salinity change, shell valves will either remain closed causing death or acclimatization will take place (Bayne et al. 1976). Vertical stratification of the water column after storms can physically isolate benthic filter feeders located in deeper subtidal regions from the upper water column preventing grazing control (Koseff et al. 1993). Under these conditions little phytoplankton is mixed down to benthic subtidal filter feeders and phytoplankton can accumulate in the upper water column. The relative influence of grazing by filter-feeding bivalves on estuarine phytoplankton dynamics after storms is dependent on their ability to withstand osmoregulatory stress and their depth in the water column.

The pygmy mussel, *Xenostrobus securis*, is an epifaunal mytilid found in high abundance on firm substrates in the intertidal zone of estuaries throughout southern Australia. The adult stage is persistent and dominant along the tidal section of estuaries and can tolerate a wide range of salinities, actively filtering when salinities are between 5 and 32.5 psu (Wilson 1968; Wilson 1969). Its unusually wide salinity tolerance and physiological ability to withstand sudden osmotic shock, combined with an intertidal habitat among mangrove pneumatophores, may allow *X. securis* to exert top-down control of phytoplankton blooms, even when salinities have dropped considerably and when the water column has become vertically stratified.

Mass balance techniques quantify inputs and outputs to a system to determine hydrodynamic transports and the bulk fluxes of biogeochemically active elements such as nitrogen and phosphorus in estuarine systems (Smith and Atkinson 1983; Smith and Veeh 1989). In this earlier work, biological mechanisms resulting in a net uptake or release of the nutrient are inferred to account for nonconservative fluxes in the system. Coupling these transports with a biological model would allow a quantitative analysis of the relative importance of hydrodynamic and biological mechanisms and identify the sources and sinks within a system.

In this study a process-oriented approach is undertaken to quantify the influence of hydrodynamic processes, nitrogen limited phytoplankton growth, and grazing by the mussel *X. securis* on phytoplankton bloom dynamics in the weeks following a storm using a simple one-dimensional hydrodynamic-ecological box model. A salt balance is used to approximate the longitudinal dispersion coefficients from observations. A biological model with nitrogen limited phytoplankton growth, mussel grazing, and a phytoplankton mortality term is forced by the calculated transports. A consideration of the individual terms in the model equations is used to quantify the relative importance of hydrodynamics, phytoplankton growth, mussel grazing, and other biological loss terms on the development of the bloom. Simulations with variations of the maximum phytoplankton growth rate, mussel grazing rates, and phytoplankton mortality coefficient shed light on the robustness of conclusions and point to where future research would be most profitably directed.

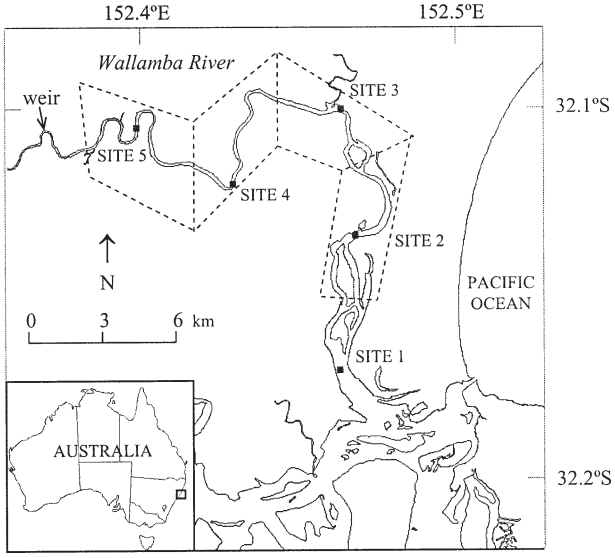

Fig. 1. Wallis Lake region with Wallamba River sampling sites (dots), model box boundaries, and the location of the weir.

Study Location

The Wallamba River is a subtropical estuary that flows into the entrance area of Wallis Lake, a permanently open coastal lagoon on the mid-north coast of New South Wales, Australia (Fig. 1). Of the four estuaries that drain the Wallis Lake catchment, the Wallamba River has the largest subcatchment covering approximately 500 km^2 or one third of the entire catchment (1440 km^2). Approximately 70% of the subcatchment has been extensively cleared and is primarily used for cattle grazing and dairy farming.

The Wallamba River experiences a semidiurnal tidal cycle that extends approximately 28 km upstream at which point it is restricted by a weir. The mean tidal amplitude is 0.27 m and the horizontal tidal excursion is 3.75 km on the flood tide and 2.25 km on the ebb tide (Allsop and Kadluczka 1999). The region is without large seasonal contrasts in rainfall, but mostly experiences a summer rainfall regime with the wettest month usually in March and the driest month usually in September.

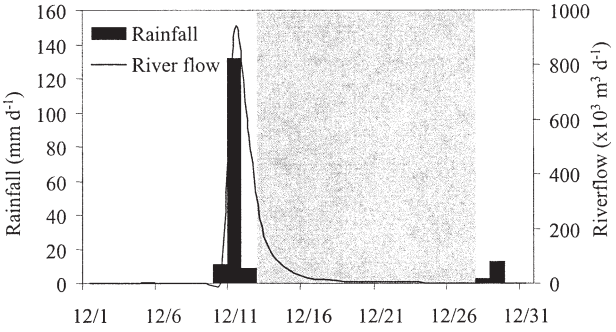

Fig. 2. Daily rainfall for the Wallamba River catchment and daily river flow during December 2002. The shaded area represents the sampling period from day 2 until day 16 after the storm on December 11, 2002. Dates are month/day. Source: Bureau of Meteorology station no. 60021.

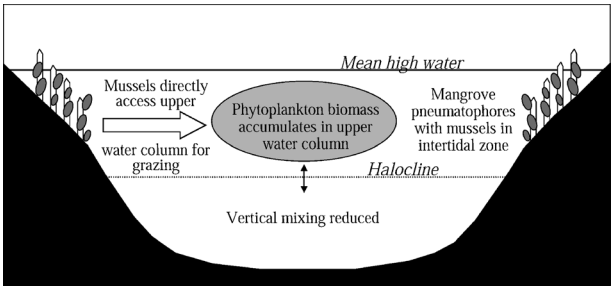

Fig. 3. Conceptual diagram showing the accumulation of phytoplankton biomass in the upper water layer under stratified conditions. Light and nutrient conditions are favorable in the upper layer and vertical dispersion cannot overcome strong density gradients to mix phytoplankton down to the bottom waters. *Xenostrobus securis* on mangrove pneumatophores in the intertidal zone can directly access the upper water column and graze the phytoplankton from the lateral boundaries. Assuming strong horizontal mixing, *X. securis* may exert top-down control on the bloom. Other biological loss processes, such as coagulation and sinking, are not shown.

Materials and Methods

Sampling and Analytical Methods

Five sites approximately 4 km apart along the Wallamba River (Fig. 1) were sampled after a storm on December 11, 2002, when 132 mm rain fell in 24 h, representing approximately 10% of the average annual rainfall (unpublished data). The storm broke a prolonged dry period during which only 56 mm rain fell as intermittent, small showers in the three preceding months. Average daily river flow increased from < 1 to 928×10^3 m^3 d^{-1} within 24 h of the storm (Fig. 2). Sampling occurred 2, 4, 6, 9, 12, and 16 d after the storm.

Sampling took 1 to 2 h to complete and began between 0700 and 0900 h. At each site salinity was measured in situ at 1-m intervals from the surface to the depth of the water column using a Yeo-Kal 611 conductivity, temperature, and depth unit. Water samples ($n = 2$) were collected from the surface in sterile 100-ml containers for analyses of oxidized nitrogen (NO_2^- and NO_3^-) and ammonium (NH_4^+), and in darkened 2- l bottles for analyses of chlorophyll *a* (chl *a*). Water samples were kept cool and away from direct sunlight until filtering.

Water sampled for nutrient analyses was filtered through a sterile disposable 0.45-μm syringe filter into a 30-ml vial and stored at −20°C. Nutrient concentrations were determined using the American Public Health Association Method 4500 (Standard Methods for the Examination of Water and Wastewater unpublished data) modified for NO_2^- + NO_3^- and NH_4^+ on the Lachat Instruments autoanalyzer. The Practical Quantitation Limits of this method are 0.07 and 0.14 μmol l^{-1} for NO_2^- + NO_3^- and NH_4^+, respectively.

Water sampled for chl *a* analysis was filtered through a 47-mm diameter, 1.2-μm glass fiber filters under low vacuum within 7 h of collection. Filters were then folded, blotted dry, wrapped in aluminium foil, and stored at −20°C until analysis. Chl *a* concentration was calculated using the method of Jeffrey and Humphrey (1975).

Model Development

A conceptual model illustrating the hypothesis that intertidal epifaunal mussel grazing by *X. securis* can regulate phytoplankton biomass accumulation in the upper layer of a stratified water column after a storm is shown in Fig. 3. Light and nutrient conditions are favorable for phytoplankton growth in the upper layer and vertical dispersion is inhibited by strong density gradients, resulting in little dilution of phytoplankton by the bottom waters. The mussel *X. securis* on mangrove pneumatophores in the intertidal zone can directly access the upper water column and graze phytoplankton from the lateral boundaries. Assuming strong cross-stream mixing, *X. securis* may exert top-down control on the bloom.

Water transports in the upper water column of a 20 km stretch of the Wallamba River were examined using a one-dimensional box model and by solving mass balance equations for salt. The salt-balance method for box models requires knowledge of the estuarine geometry and freshwater inputs to estimate nonadvective transports (diffusion and dispersion) between boxes using the observed distribution of salt. Because salt is a conservative tracer these estimated transports encompass all mixing processes including those driven by temperature and salinity gradients, wind, and tides. Salt, and any other observable property, is considered to be homogenously distributed within each box. Mixing of properties occurs only between boxes that share a common interface (Officer 1980). This

TABLE 1. Dimensions of model boxes.

Box geometry (m)	Box 5	Box 4	Box 3	Box 2
Length	3362.24	3644.38	3664.70	4608.40
Width	66.87	89.48	116.58	166.72
Depth	1.50	1.50	1.50	1.63

results in n linear mass balance equations that can be solved simultaneously for n unknown nonadvective transports. In this study, salt-balance equations were solved using salinity observations for each day sampled and then used to calculate water transports to force the box model.

The estuary was divided into 4 boxes with the most upstream model box (Box 5) surrounding sampling Site 5 and the most downstream model box (Box 2) surrounding Site 2. The upstream and downstream boundaries of each box were calculated using the linear mid points between adjacent sites. The distance between a site and its upstream boundary is approximately equal to the distance between the upstream boundary and the next upstream site. This means that the sites are not centered exactly in the middle of each model box; rather the model box boundaries are equidistant between sites. The volumes of model boxes were determined using spatially resolved bathymetric data (Department of Infrastructure, Planning and Natural Resources unpublished data) consisting of depth measurements at 5-m intervals along cross-sectional transects at longitudinal distances of 200 to 500 m along the estuary. The horizontal area of each box was determined from the average width of the estuary multiplied by the longitudinal distance between box boundaries. The depth of each model box was determined by the position of the halocline and was multiplied by the horizontal area to give the model box volumes. Model box geometry is given in Table 1.

All freshwater inputs enter at the head of the estuary and were approximated using a conversion table from automated river height measurements made 4 km upstream of Site 5 on the upstream side of a weir. Historical measurements from 1969 to 1978 covering a range of conditions from zero flow to flood events with discharges of up to 85 $\times$ 10^6 m^3 d^{-1} were used to create the conversion table (Department of Infrastructure, Planning and Natural Resources unpublished data). Because the river height measurements were made on the upstream side of a weir, the corresponding volume of water discharged into the estuary is fresh. This measure of flow into the system is representative of advective transport, R (m^3 d^{-1}), and is used to determine the cross-sectional mean velocity for the mass balance equations below.

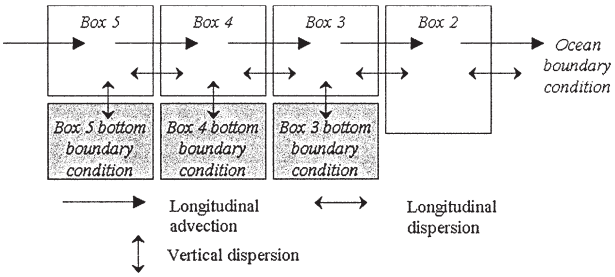

Fig. 4. Salinity profiles with depth for each day sampled after the storm for Sites 5, 4, 3, and 2 within the Wallamba River.

The longitudinal nonadvective transports were calculated for all boxes using a least squares optimization method in Matlab (fsolve) for each day sampled by solving the salt-balance equation

$$\frac{\partial s}{\partial t} = -u\frac{\partial s}{\partial x} + \frac{\partial}{\partial x}\left(K_x\frac{\partial s}{\partial x}\right) + \frac{\partial}{\partial z}\left(K_z\frac{\partial s}{\partial z}\right) \quad (1)$$

where s is salinity (psu), t is time (d), u is the cross-sectional mean longitudinal velocity (m d^{-1}), x is the longitudinal position in the estuary and is positive downstream (m), K_x is the longitudinal dispersion coefficient (m^2 d^{-1}), z is the position in the water column and is positive with depth (m), and K_z is the vertical dispersion coefficient (m^2 d^{-1}). The first term on the right hand side of Eq. 1 assumes constant longitudinal advection downstream and no estuarine circulation or upstream transport in the bottom layer (see discussion of Fig. 4). The usual assumption that salinity is at steady state cannot be used here because of the rapid recovery of salt to the upper water column following the storm. This assumption has been relaxed and an additional term is included in the equations reflecting the time-rate-of-change of salinity, $\partial s/\partial t$. For systems that have been sampled at high frequency (days to weeks), the inclusion of a time varying term for conservative tracers, or tendency term, can improve circulation estimates (Roson et al. 1997; Hagy et al. 2000). Here tendency is calculated as the change in salinity of the model boxes over the period of two sampling days.

A further modification on the usual one-dimensional box model in this study is the inclusion of a vertical dispersion term for boxes corresponding to sites with a strong halocline. Assuming longitudinal transports in the bottom layer are negligible, vertical transport was calculated as

$$D_z = \frac{(s_{Bt+1} - s_{Bt-1})z_B A}{\Delta t \partial s} \quad (2)$$

where $s_{Bt+1} - s_{Bt-1}$ is the change in salinity of the bottom waters over a period of two sampling days, z_B is the thickness of the bottom waters from which salt

is being depleted (m), A is the horizontal area over which dispersion occurs (m^2), Δt is the period of time between the two sampling days (d), and ∂s is the concentration gradient of salt between the upper and bottom waters at time t. The term $(s_{Bt+1} - s_{Bt-1})z_B A$ of Eq. 2 is the total amount of salt depleted from the bottom waters dispersed into the upper model boxes over the time period Δt. The units of D_z are $m^3\ d^{-1}$. The vertical dispersion coefficient is calculated as

$$K_z = \frac{D_z \Delta z}{A} \tag{3}$$

where Δz is the distance over which vertical dispersion occurs (m).

To summarize the model transports as seen in Fig. 5, the most upstream Box 5 directly receives all freshwater inputs, the volume of which determines longitudinal advection for all boxes. Longitudinal dispersion occurs at the boundaries of Boxes 2 to 5 except at the upstream boundary of Box 5. For boxes corresponding to sites with a strong halocline (Boxes 3 to 5), vertical dispersion occurs across the bottom boundaries. To keep the model to one dimension these bottom boxes are not dynamically modelled and instead a time varying bottom boundary condition is specified. A bottom boundary condition is not applied to Box 2 because the full depth of water column was observed to be well mixed at Site 2 throughout the sampling period.

The time-rates-of-change of model nitrogen concentration and phytoplankton biomass were determined as the sum of advection, longitudinal and vertical dispersion, nitrogen uptake by phytoplankton for growth, mussel grazing, and a quadratic mortality term according to

$$\frac{\partial N}{\partial t} = -u\frac{\partial N}{\partial x} + \frac{\partial}{\partial x}\left(K_x \frac{\partial N}{\partial x}\right) + \frac{\partial}{\partial z}\left(K_z \frac{\partial N}{\partial z}\right) - \frac{\mu_{max} B N}{K_N + N} \tag{4}$$

and

$$\frac{\partial B}{\partial t} = -u\frac{\partial B}{\partial x} + \frac{\partial}{\partial x}\left(K_x \frac{\partial B}{\partial x}\right) + \frac{\partial}{\partial z}\left(K_z \frac{\partial B}{\partial z}\right) + \frac{\mu_{max} B N}{K_N + N} - \alpha B - \phi B^2 \tag{5}$$

where N is the concentration of dissolved inorganic nitrogen (DIN = $NO_3^- + NO_2^- + NH_3$; μmol N l^{-1}), μ_{max} is the maximum phytoplankton growth rate (d^{-1}), B is phytoplankton biomass as the concentration of nitrogen (μmol N l^{-1}), K_N is the half-saturation constant for growth as a function of nitrogen and is the value of N at which $\mu = \frac{1}{2}\mu_{max}$ (μmol N l^{-1}), α is the mortality rate of phytoplankton due to grazing by *X. securis* as discussed below (d^{-1}), and ϕ is the coefficient of the quadratic mortality term (l μmol N^{-1} d^{-1}). It is assumed that the light climate remains constant throughout the simulation, so the estimated value of μ_{max} is a depth integrated maximum growth rate for the standard light conditions in the upper water column. This is reasonable as only the upper water column is modelled, reducing the influence of self-shading as the bloom progressed.

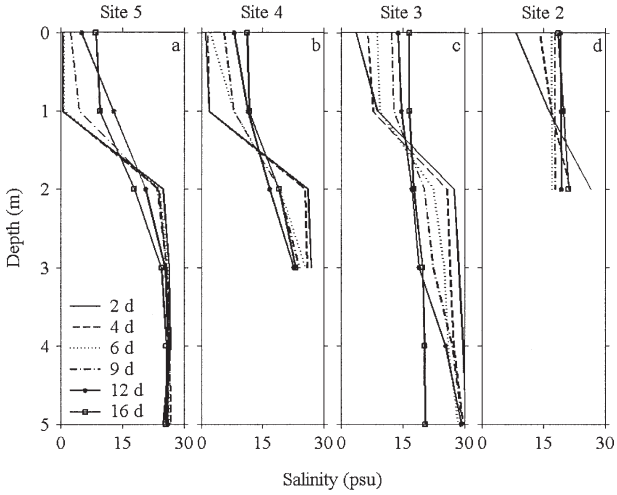

Fig. 5. Schematic diagram of the model summarizing the advective and dispersive mechanisms influencing salinity, nitrogen concentration, and phytoplankton biomass. The shaded bottom boxes are not directly included in the model keeping it to one dimension, but properties can disperse vertically across the boundary between the top and bottom boxes.

The maximum phytoplankton growth rate is estimated to be ln (2) = 0.69 d^{-1}, which is one doubling per day, based on previously determined values of μ_{max} for selected species (Graham 2000). The robustness of conclusions from simulations using this value of μ_{max} is assessed by varying it by factors of ± 2. The half-saturation constant for nitrogen is 1 μmol N l^{-1} following previous work on nutrient transformation and phytoplankton growth in other subtropical east Australian estuaries (Eyre 2000).

A conversion factor of 1.59 g chl *a* (mol N)$^{-1}$ was used to compare model phytoplankton nitrogen with chl *a* observations, calculated from 0.02 g chl *a* (g C)$^{-1}$ for open ocean phytoplankton (Fasham et al. 1990) and the Redfield ratio C:N = 106:16 (Redfield et al. 1963).

The nitrogen and phytoplankton concentrations of the freshwater input flowing directly into the most upstream Box 5 remain constant throughout the model simulations. Freshwater nitrogen concentration was set to the observed value at Site 5 on

TABLE 2. Advective transports (R) and longitudinal (K_x) and vertical (K_z) dispersion coefficients calculated for each day sampled after the storm and used to force the dynamic box model.

		K_x ($\times 10^6$ m^2 d^{-1})				K_z ($\times 10^{-2}$ m^2 d^{-1})		
Day	R ($\times 10^3$ m^3 d^{-1})	Box 5	Box 4	Box 3	Box 2	Box 5	Box 4	Box 3
2	168.21	0.38	0.53	1.68	4.79	1.43	1.76	3.03
4	38.21	1.15	2.07	1.38	1.67	0.48	1.40	3.90
6	12.38	1.72	4.13	2.83	1.73	0.10	1.84	4.57
9	4.48	4.23	2.96	3.71	1.97	1.36	2.57	7.45
12	2.49	11.64	2.56	2.91	1.67	1.70	3.08	8.37
16	1.87	0.04	0.49	3.47	1.10	0.59	4.07	0.96

the first sampling occasion 2 d after the storm. The large pulse of freshwater delivered to the estuary in the few days after the storm is assumed to be derived from land runoff with very low concentrations of freshwater species of phytoplankton. The phytoplankton concentration of the freshwater input is set to zero throughout the simulations.

The ocean boundary conditions applied at the downstream boundary of Box 2 were time varying throughout the model simulations. Ocean conditions were the observed values of salt, nitrogen, and chl *a* at the most downstream site (Site 1) on each sampling occasion. These values were linearly interpolated over time and dispersed longitudinally with the simulated properties of Box 2.

The bottom flux boundary conditions applied to Boxes 3 to 5 where a strong halocline was observed were also time varying throughout the model simulations. The vertical dispersion of salt into the upper boxes was determined from observations made during the sampling period as described above (Eqs. 2 and 3). This vertical dispersion coefficient was used to calculate the flux of nitrogen and chl *a* across the bottom boundaries of Boxes 3 to 5. Because nitrogen and chl *a* were measured only at the surface during the sampling period, the concentrations of these properties in the bottom boxes were set to values observed shortly prior to the storm on December 5, 2002. This was done because the freshwater input to the estuary after the storm formed an upper layer overlying the well-mixed water mass present before the storm (see Fig. 4). As such, it was assumed that the bottom waters at each site had retained similar properties to those observed at the surface shortly prior to the storm. This assumption is supported by salinity observations at depth from each site at the beginning of the storm sampling period closely matching observations from December 5, 2002.

The box model was forced dynamically using the transports R, D_x, and D_z linearly interpolated over time (Table 2). The ocean boundary DIN and chl *a* concentrations and the DIN and chl *a* flux boundary conditions applied to the bottom of Boxes 3 to 5 are given in Table 3. The dynamic model employed a 4–5th order Runge-Kutta integration method with a relative tolerance of 10^{-9} to solve the differential equations at each time step for salt, nitrogen, and phytoplankton. Initial conditions for the model are the observed day 2 values of salinity, DIN, and chl *a*.

The abundance and distribution of *X. securis* in the Wallamba River is approximated using the area of mangrove pneumatophores on the riverbank in the intertidal zone that they inhabit. The habitat area is calculated using aerial photography and taking an approximate width of 0.75 m of mangrove pneumatophores where *X. securis* occur (Moore personal observation). The areas of pneumatophores are 6,678, 1,552, and 3,292 m^2 for Boxes 2, 3, and 4, respectively.

The clearance rate of *X. securis* has not been determined and is instead approximated by applying the clearance rates of the zebra mussel, *D. polymorpha*. Although *D. polymorpha* is a freshwater species, it is a similarly sized epifaunal mytilid. Small (9–11 mm mean shell length), medium (13–15 mm), and large (19–22 mm) *D. polymorpha* have been found to remove chl *a* at average rates of 58,

TABLE 3. Ocean boundary dissolved inorganic nitrogen (μmol l^{-1}) and chlorophyll *a* (mg m^{-3}) concentrations and the dissolved inorganic nitrogen ($\times 10^3$ μmol m^{-2} d^{-1}) and chlorophyll *a* (mg m^{-2} d^{-1}) flux boundary conditions applied to the bottom of Boxes 3 to 5.

	Concentration boundary condition	Flux boundary condition		
Day	Ocean	Bottom Box 5	Bottom Box 4	Bottom Box 3
Dissolved inorganic nitrogen				
2	5.1	−3.33	−3.83	−3.36
4	4.6	−1.12	−3.05	−4.37
6	4.4	−0.18	−2.93	−3.41
9	3.4	−1.13	−2.37	−2.95
12	1.9	−0.43	−1.49	−1.71
16	3.9	−0.07	−0.41	−0.07
Chlorophyll *a*				
2	3.1	95.91	64.31	32.88
4	2.3	9.44	28.68	−292.18
6	3.2	−26.06	−581.70	−1167.80
9	3.6	−1156.70	−742.26	−876.73
12	3.0	−535.93	−553.30	−603.89
16	1.6	−19.14	31.26	−39.66

110, and 232 ml mussel^{-1} h^{-1}, respectively (Kryger and Riisgard 1988; Horgan and Mills 1997). A power relationship was fit to predict clearance rate (CR) from shell length (SL) and was applied to size specific distribution and abundance data for *X. securis* from mangrove pneumatophore habitat in the Wallamba River (CR = 0.65 × SL$^{1.94}$). *X. securis* data were collected monthly from December 2001 to April 2002 for a concurrent study (Giles 2002). Data are the average of three 0.04-m^2 quadrats of pneumatophores collected to root level at 6 sites in the Wallamba River and included mussels in 34 size classes up to a length of 34 mm. Approximated areal clearance rates for the size structure and abundance of the *X. securis* populations at Sites 2, 3, and 4 are 19.4, 51.4, and 16.1 m^3 m^{-2} d^{-1}, respectively. Areal clearance rates are multiplied by the area of mangrove pneumatophores on the riverbank within each model box and divided by the volume of corresponding model boxes to give the mortality rates of phytoplankton due to grazing by *X. securis* of 0.10, 0.12, and 0.11 d^{-1} for Boxes 2, 3, and 4, respectively. A mortality rate due to mussel grazing was not applied to the most upstream box (Box 5) as no significant mangrove beds occur within its boundaries. Two conditions were imposed on the mortality rates for the model simulations; *X. securis* only grazed when salinities were > 5 psu (Wilson 1968), and grazing was inhibited for 6 h d^{-1} at low tide when mangrove pneumatophores were exposed.

The least known of the parameters in Eqs. 4 and 5 is the coefficient of the quadratic mortality term, ϕ. This quadratic mortality term represents phytoplankton loss processes in the water column other than advection, dispersion, and *X. securis* grazing, such as endogenous respiration, nonpredatory mortality, settling, and grazing by zooplankton. Unlike the mussel grazing parameter, which is based on a combination of field observations of mussel abundance and laboratory experiments, we have no independent estimation of the quadratic mortality term's likely value in Wallamba River. As the least known parameter, its value was adjusted in order to obtain a good fit between model and observed phytoplankton biomass. This approach is commonly taken for higher order closure terms in plankton models (Steele and Clark 1998). Achieving a good fit between model and observed phytoplankton biomass will be particularly important when comparing the relative magnitude of the phytoplankton terms, all of which are a function of phytoplankton biomass.

An additional six model simulations were conducted with the maximum phytoplankton growth rate, the total grazing by *X. securis*, and the coefficient of the quadratic mortality term varied by factors of ± 2. The additional simulations indicate the sensitivity of model results to uncertainty in the estimation of the maximum phytoplankton growth rate, the *X. securis* grazing rate, and the quadratic mortality term.

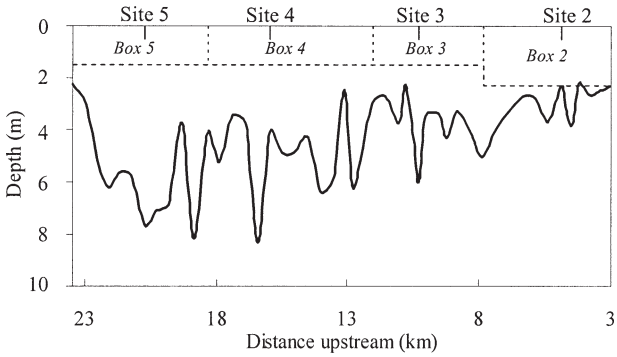

Fig. 6. Maximum cross-sectional depth of the Wallamba River plotted against distance upstream from Site 1 at the mouth of the estuary. Sampling site locations and model box boundaries are shown. Source data: Department of Infrastructure, Planning and Natural Resources.

Results

Observations

Increased river flow resulted in a pulse of freshwater between 1 and 2 m thick overlying prestorm water for Sites 3 to 5 (Fig. 4). The halocline was taken to be at 1.5 m depth and this becomes the depth of model Boxes 3 to 5. Salinity measurements at Site 2 showed no persistent stratification over the sampling period indicating extensive overturning of the water column. The depth of Box 2 is 1.63 m, which is the average depth within the box domain from bathymetry data. The volume of the model boxes becomes 12.5, 6.4, 4.9, and 3.4 × 10^5 m^3 for Boxes 2, 3, 4, and 5, respectively. Longitudinal advection and dispersion are inhibited in the subsurface layer due to the highly uneven bathymetry of the Wallamba River with numerous ridges acting as physical barriers (Fig. 6). This is evident by the lack of a salt wedge structure penetrating upstream at depth. The salinity measurements at the bottom of the deeper Sites 3 and 5 remain relatively unchanged during the sampling period. An exception to this occurs at Site 3 on day 16, when the water column is vertically well mixed from surface to depth. Because this occurs only on the last day of the sampling period it does not influence the model simulation to that point. Bottom salinities at Site 4 are more variable due to the shallower water depth, but they become fresher with time, which is inconsistent with a salt wedge and estuarine circulation. Salinities at Sites 3 to 5 at 2 m depth just below the halocline became

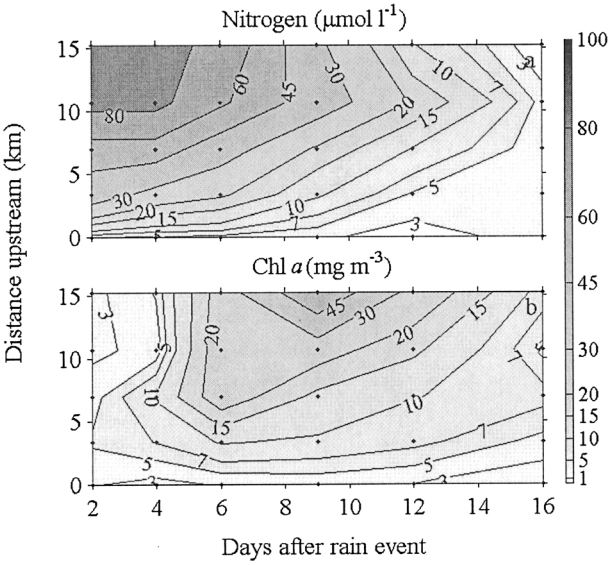

Fig. 7. Contoured observed dissolved inorganic nitrogen and chlorophyll *a* (chl *a*) at the surface during the sampling period with distance upstream from Site 1 for the Wallamba River. The points in time and space where observations were made are indicated by black dots and represent the five sites on each day sampled.

fresher with time as the halocline gradually weakened and the upper layer became saltier. This indicates that vertical dispersion is a mechanism delivering salt to the surface waters.

DIN concentrations of 90 μmol l^{-1} are associated with the pulse of freshwater observed 2 d after the storm at Site 5 (Fig. 7). Nitrogen concentrations are highest furthest upstream for the entire sampling period indicating that the main source of this nutrient is from the river draining the upper catchment with comparatively small inputs along the estuary. The initial high concentrations of nitrogen begin to decline by day 6 corresponding with an increase in chl *a*. Chl *a* remains low at 2.3–5.3 mg m^{-3} for all sites for the first 4 d. After this time chl *a* begins to increase peaking at 58.5 mg m^{-3} at the most upstream Site 5 on day 9. The highest concentrations of chl *a* are observed furthest upstream for each day sampled.

Model Results

When the nonadvective transport terms approximated from the salt balance were interpolated and used to simulate salinity distributions, model salinity closely matched observations (Fig. 8). Pearson's correlation between model and observed salinity for Boxes 2 to 5 over the 16-d sampling period shows good agreement (r = 1.0, n = 24), as would be expected using the inverse methods of obtaining D_x. This indicates that the transport terms for a passive tracer are well approximated by the box model.

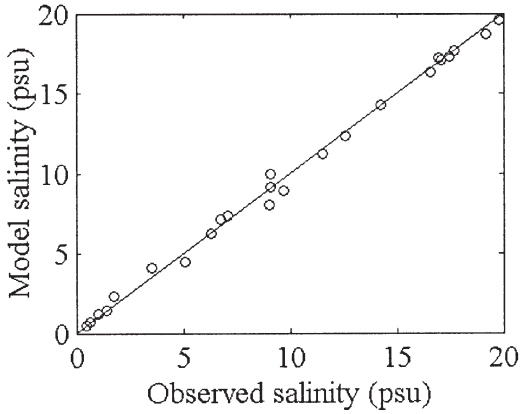

Fig. 8. Observed surface salinity for Sites 2, 3, 4, and 5 plotted against model salinity for Boxes 2, 3, 4, and 5 for each day sampled. The solid line represents the 1:1 line for comparison.

The quadratic mortality term was adjusted to obtain a good fit between observed and modelled chl *a* biomass and was found to take a value of 0.015 l μmol N^{-1} d^{-1}. Model and observed nitrogen correlate well for the simulation (r = 0.98, n = 24; Fig. 9). The ability of the model to predict the temporal and spatial patterns of phytoplankton biomass is slightly less for nitrogen (r = 0.82, n = 24). Model chl *a* peaks at upstream sites after approximately 9.6 d and agrees with the timing and location of the observed chl *a* peak at 9 ± 2 d (Fig. 10). The residuals of chl *a* (model minus observed values) show that the model slightly underestimates chl *a* in the upstream box and overestimates chl *a* in the middle two boxes from days 6 to 12. The error is small compared to the magnitude of the observations.

An examination of the model terms contributing to the net gain or loss of phytoplankton in each box throughout the sampling period reveals that phytoplankton biomass is primarily driven by local biological processes (Fig. 11). Phytoplankton growth reaches a maximum rate of 17.3, 23.1, 28.2, and 32.6 mg chl *a* m^{-3} d^{-1} at approximately day 9 for Boxes 2, 3, 4, and 5, respectively. The timing varies slightly with location, being generally earlier downstream due to quicker nutrient depletion. This time also closely corresponds to when the highest model chl *a* is observed for all boxes. The highest rates of growth occur furthest upstream following the spatial trend in nitrogen concentrations. After the phytoplankton biomass peaks at 9.6 d nitrogen becomes limiting and growth rapidly decreases. Mussel grazing losses from Boxes 2 and 3 gradually increase to −2.4 and −3.5 mg chl *a* m^{-3} d^{-1} at approximately day 8.5. For Box 4, mussel grazing pressure is non-zero only after day 4 when salinities are > 5 psu, and reaches a maximum

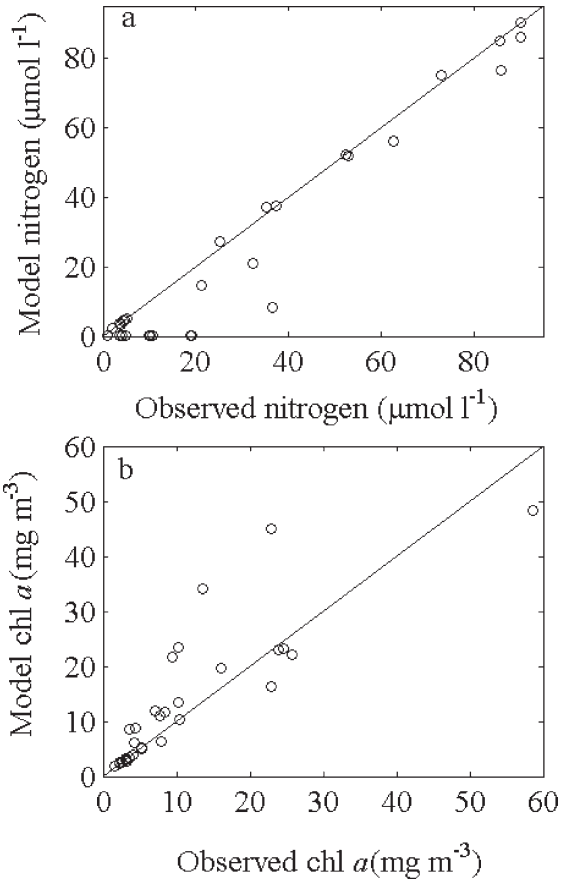

Fig. 9. Observed dissolved inorganic nitrogen and chlorophyll *a* (chl *a*) for Sites 2–5 plotted against model values for Boxes 2–5 for each day sampled. The solid line represents the 1:1 line for comparison.

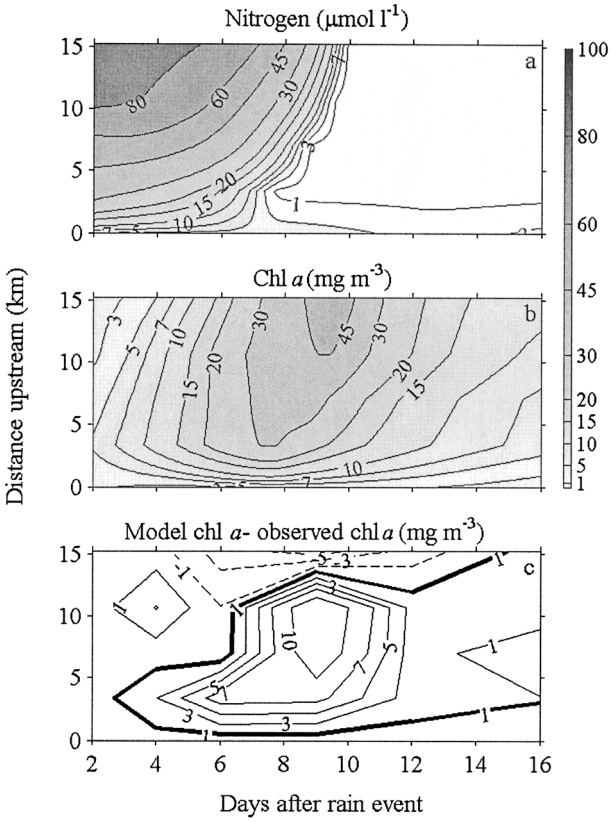

Fig. 10. Model dissolved inorganic nitrogen, chlorophyll *a*, and model minus observed chlorophyll *a* during the sampling period with distance upstream from Site 1.

rate of loss of −3.7 mg chl *a* m^{-3} d^{-1} at 9.3 d. Mussel grazing losses then gradually decrease for the remainder of the simulation and are directly related to phytoplankton biomass for Boxes 2 to 4. The rates of change of phytoplankton biomass due to advective and dispersive mechanisms are mostly less than the biological mechanisms for each box, and are in fact up to an order of magnitude less compared to growth rates. Vertical dispersion, which is calculated based on salt lost from below the surface boxes (Eq. 2), is a small term ranging from 0 to −2.5 mg chl *a* m^{-3} d^{-1} for Boxes 3 to 5 throughout the simulation, suggesting a more sophisticated representation of vertical mixing is not necessary. The differences between the sum of physical and biological processes and modelled tendency (local rate of change) are $< 0.1\%$ for the estuary, indicating that the model conserves mass and there are no spurious sources or sinks of nitrogen or phytoplankton due to equation discretization.

Sensitivity Analysis

Model nitrogen and chl *a* were sensitive to variations in the maximum phytoplankton growth rate, μ_{max}. Model nitrogen was depleted much less rapidly compared to the original simulation when μ_{max} was decreased by a factor of 2 and more closely matched observed nitrogen values (Fig. 12). Model chl *a* was slow to bloom and was still increasing at day 16. The timing of the bloom occurs $>$ 7 d later compared to the simulation using the original values for these parameters and to observations. Although the influence of phytoplankton growth is considerably reduced reaching only 4.7, 5.4, 7.0, and 9.0 mg chl *a* m^{-3} d^{-1} for Boxes 2, 3, 4, and 5, respectively, on day 16, phytoplankton dynamics are primarily driven by growth for the duration of the sampling period (Fig. 13). Because the biomass of phytoplankton during the sampling period was greatly reduced, all loss terms including grazing by *X. securis* for Boxes 2, 3, and 4 exerted less of an influence on phytoplankton dynamics.

Increasing μ_{max} by a factor of 2 resulted in model nitrogen being depleted more rapidly and model

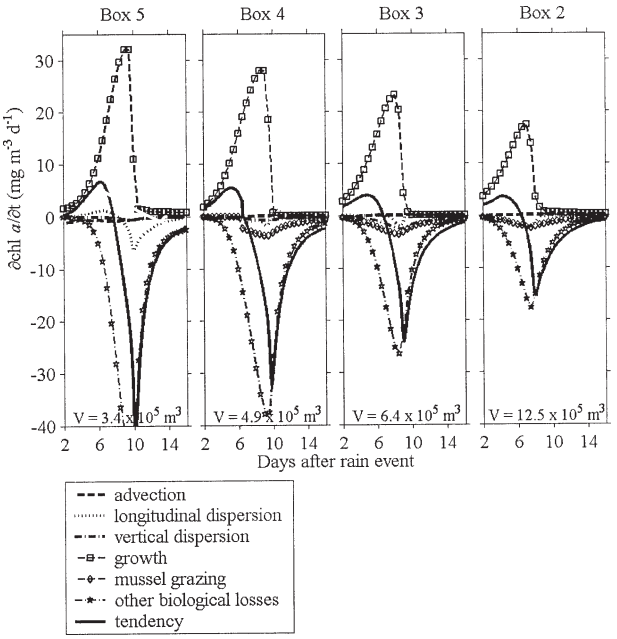

Fig. 11. Rate of change of model chlorophyll *a* due to hydrodynamic and biological mechanisms for Boxes 5, 4, 3, and 2 during the sampling period. Hydrodynamic processes derived from the mass balance equation are advection, longitudinal dispersion, and vertical dispersion. Biological processes are phytoplankton growth, phytoplankton mortality due to grazing by *Xenostrobus securis* when salinity > 5 psu, and other biological losses parameterized using a quadratic term. Tendency is the time rate of change of model chlorophyll *a* and is the sum of both the hydrodynamic and biological terms.

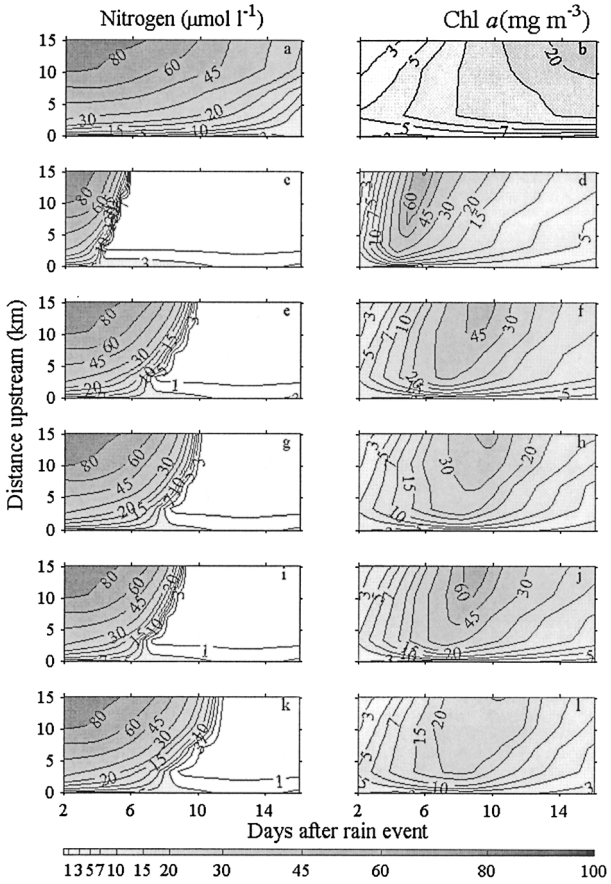

Fig. 12. Model output from the sensitivity analysis showing model nitrogen and chlorophyll *a* with the maximum phytoplankton growth rate decreased by a factor of 2, maximum phytoplankton growth rate increased by a factor of 2, *Xenostrobus securis* grazing decreased by a factor of 2, *X. securis* grazing increased by a factor of 2, quadratic loss term decreased by a factor of 2, and quadratic loss term increased by a factor of 2.

chl *a* blooming earlier compared to the simulation using the original values for these parameters and to observations (Fig. 12). Phytoplankton dynamics are initially dominated by growth that reached 44.9, 70.9, 93.7, and 101.6 mg chl *a* m^{-3} d^{-1} for Boxes 2, 3, 4, and 5, respectively, at day 5.7 (Fig. 13), corresponding in time with the maximum concentrations of model chl *a* at the most upstream Box 5.

Model nitrogen and chl *a* were less responsive to variations in grazing by *X. securis*. Decreasing the grazing parameter α by a factor of 2 had little influence on model nitrogen or chl *a*. The timing of the bloom peak (day 9.6) remained similar to that of the simulation using the original values for these parameters and observations. Increasing α by a factor of 2 also had little influence on model nitrogen, but reduced the magnitude of the model chl *a* bloom compared to the simulation using the original values for these parameters (Fig. 12). The timing of the peak in phytoplankton biomass (day 9.8) was also similar to that for the original simulation and observations. The magnitude of the simulated bloom was comparatively reduced, and consequently model chl *a* more closely matched observations. Mussel grazing control of phytoplankton was enhanced and reached −4.1, −5.9, and −6.6 mg chl *a* m^{-3} d^{-1} for Boxes 2, 3, and 4, respectively, on approximately day 8 (Fig. 13).

Model nitrogen and chl *a* were quite responsive to changes in the quadratic mortality term. When the quadratic mortality term was decreased by a factor of 2, a maximum chl *a* biomass of 74.6 mg m^{-3} was reached on day 9.1 (Fig. 12). This is the maximum biomass achieved in any of the simulations. The phytoplankton terms are dominated by growth and quadratic mortality terms, with the maximum quadratic mortality terms reaching −6.8, −12.1, −18.9, and −26.2 mg m^{-3} d^{-1} for Boxes 2, 3, 4, and 5, respectively (Fig. 13). Decreasing the quadratic mortality term by a factor of 2 resulted in a maximum chl *a* biomass of 30.3 mg m^{-3} (Fig. 12). The maximum quadratic mortality terms reached −8.7, −10.9, −14.6, and

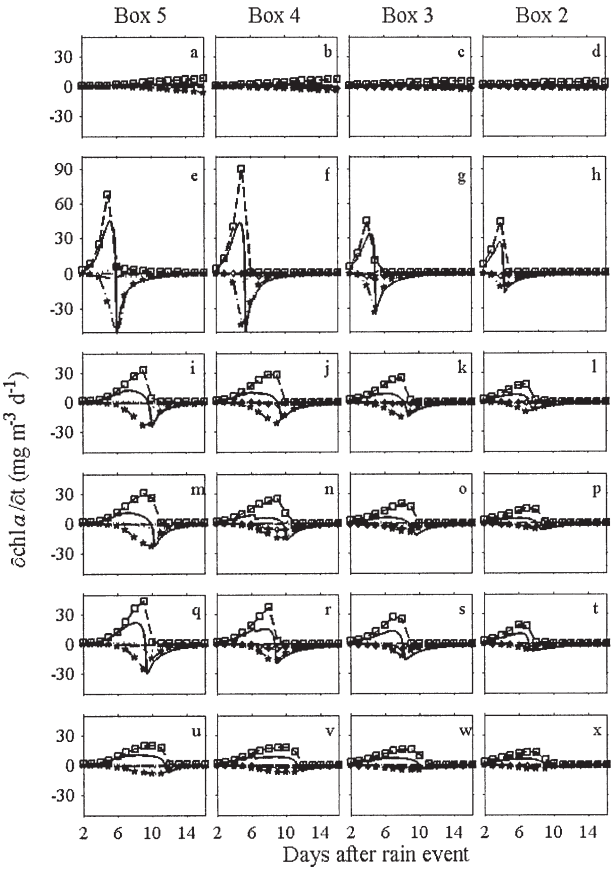

Fig. 13. Rate of change of model chlorophyll *a* due to hydrodynamic and biological mechanisms for Boxes 5 to 2 from the sensitivity analysis with the maximum phytoplankton growth rate decreased by a factor of 2, maximum phytoplankton growth rate increased by a factor of 2, *Xenostrobus securis* grazing decreased by a factor of 2, *X. securis* grazing increased by a factor of 2, quadratic loss term decreased by a factor of 2, and quadratic loss term increased by a factor of 2. Note that panels e to h have the same vertical scaling as the other panels, but extend from −40 to +100 mg m^{-3} d^{-1}. Refer to Fig. 11 for legend key.

−17.3 mg m^{-3} d^{-1} for Boxes 2, 3, 4, and 5, respectively (Fig. 13).

When model chl *a* from the sensitivity analyses was compared with observations, correlation coefficients were mostly less than for the simulation using the original parameter values of phytoplankton growth and mussel grazing (Table 4). An exception was the simulation with mussel grazing increased by a factor of 2, which produced a better overall model fit for chl *a* (r = 0.84 compared with 0.82, n = 24) for a similar fit of dissolved nitrogen. The simulation with the quadratic phytoplankton loss term increased by a factor of 2 also produced a better model fit for chl *a* (r = 0.86, n = 24), but weakened the correlation for DIN (r = 0.96 compared with 0.98, n = 24) and resulted in the phytoplankton bloom on day 5.7, occurring approximately 3 d earlier than observations.

Discussion

Model Results

This study examined the interaction between advective and dispersive mechanisms, nitrogen limited phytoplankton growth, grazing by the mussel *X. securis*, and other unidentified biological loss processes. The phytoplankton advective and dispersive terms were estimated from observed rainfall and salinity, while the *X. securis* grazing term was calculated using abundance measurements from the field. The estimation of these rates is independent of the observed chl *a* and dissolved nitrogen fields. The quadratic mortality term is based on matching the model chl *a* with the observed chl *a*.

This simple approach enables important features of the bloom dynamics to be captured with a one-dimensional box model for the Wallamba River. A breakdown of terms allows the model to be used as a diagnostic tool to better understand the cause and effect mechanisms underlying the field observations. Elevated concentrations of DIN following the storm increased phytoplankton growth and created bloom conditions in the Wallamba River. In spite of an increase in river flow from < 1 to 928×10^3 m^3 d^{-1}, the breakdown of phytoplankton terms shows advective and dispersive mechanisms did not have a strong influence on the dynamics of the bloom (Fig. 11). The biological terms of phytoplankton growth, grazing by *X. securis*, and the quadratic mortality term were a number of factors larger than the advective and dispersive terms.

Grazing by filter-feeding bivalves in other estuarine systems has only been described for benthic filter feeders that inhabit subtidal soft sediments and filter bottom waters. For these systems water column stratification can prevent grazing control of

TABLE 4. Pearson's correlation coefficients for model and observed dissolved inorganic nitrogen (DIN) and chlorophyll *a* (chl *a*) from the sensitivity analysis. The maximum phytoplankton growth rate (μ_{max}), *Xenostrobus securis* grazing (α), and quadratic loss term (ϕ) were varied by factors of ± 2. Correlation coefficients for the simulation with the original values of μ_{max}, α, and ϕ are shown for comparison.

Correlation coefficient (r)	Original	$\mu_{max} \div 2$	$\mu_{max} \times 2$	$\alpha \div 2$	$\alpha \times 2$	$\phi \div 2$	$\phi \times 2$
DIN	0.98	0.94	0.81	0.97	0.98	0.96	0.98
Chl *a*	0.82	0.12	0.40	0.81	0.84	0.86	0.78

phytoplankton blooms by physically isolating benthic filter feeders from the upper water layer. This occurs because vertical dispersion cannot overcome density gradients to mix phytoplankton down to where it can be accessed for grazing (Koseff et al. 1993). In this study *X. securis* inhabits the intertidal zone and directly accesses the upper water layer for feeding. Stratification of the water column caused by increased freshwater inflow does not prevent *X. securis* from grazing phytoplankton in the upper water layer (Fig. 3).

Local attributes of coastal systems can be important in regulating the effects of anthropogenic nutrient enrichment (see Cloern 2001 for review), but few studies have examined interactions between the hydrodynamic and biological attributes (e.g., Lucas et al. 1999a,b). The relative importance of the different biological and physical processes throughout the flood event can be estimated by comparing the integrated value of the processes over the simulation. On day 2 the surface layer of the estuary contained 159×10^6 mol N as DIN and phytoplankton biomass. From day 2 to 16, nitrogen entering the estuary from river inflow totals 27.6×10^6 mol N. During the simulation, 28.1×10^6 mol N was consumed by *X. securis*, while other biological processes, represented by the quadratic mortality term, removed 94.6×10^6 mol N. A further 17.5×10^6 mol N is lost from model Boxes 3 to 5 through vertical dispersion, leaving 12.6×10^6 mol N as DIN and phytoplankton biomass remaining in the surface waters on day 16. Of the 186.6×10^6 mol N that was either in the estuary at day 2 or entered between day 2 and 16, only 19% left the estuary through physical transport processes, while 66% was consumed by *X. securis* grazing and other biological loss processes. *X. securis* grazing accounted for 23% of the biological processes. This analysis suggests that under these conditions *X. securis* may be an important biological attribute of the Wallamba River acting as a sink for anthropogenic nutrients.

Due to the tolerance of *X. securis* to low salinities, top-down grazing control of phytoplankton was only inhibited at the most upstream limit of their distribution at Site 4 until day 4 when they were exposed to salinities > 5 psu. Longitudinal dispersion with ocean waters and vertical dispersion with bottom waters resulted in a rapid recovery of salt to the upper water column, allowing mussels to resume filtering shortly after the storm. A larger storm resulting in a freshwater flush of the entire water column would inhibit mussel grazing over much larger spatial and temporal scales prolonging the phytoplankton bloom in the estuary.

Given the potential for *X. securis* to act as a nutrient sink after storms, management of estuarine nutrient enrichment should acknowledge the importance of mangrove habitat for the mussel and consider the long-term sustainability of this sink. Nitrogen removed from the water column and incorporated into the tissues of *X. securis* is retained within the estuary as mussel biomass. Unless mobile predators of *X. securis*, such as fish, are removing mussel biomass from estuaries it may also ultimately result in increased organic matter loads to sediments. Excessive loading of organic matter to sediments, particularly of carbon, reduces denitrification efficiencies and can result in a net release of DIN back into the overlying water column sustaining further phytoplankton growth (Heggie et al. 1999).

Assumptions and Other Factors

Although the hydrological component of the model is well addressed, the maximum phytoplankton growth rate and grazing by *X. securis* were not explicitly determined for this study. Possible errors associated with estimating growth include light limitation due to self-shading under bloom conditions and increased concentrations of suspended particulate matter after the storm, unknown species composition of phytoplankton, and possible salinity-driven changes in phytoplankton species composition in the modelled estuary domain during the sampling period. Grazing rates of *X. securis* were derived from those of *D. polymorpha* and the influence of various physiological and environmental conditions on these rates were limited. Mussel grazing rates will vary not only as a function of size as considered here, but also due to the absolute (Smaal and van Stralen 1990; Figueiras et al. 2002) and relative concentrations of phytoplankton and seston (Figueiras et al. 2002) and increased concentrations of storm-induced suspended solids at the beginning of the sampling period, current flow (Fréchette and Bourget 1985), and temperature (Aldridge et al. 1995; Babarro et al. 2000a). The influence of salinity on grazing rates has been simplified here by preventing grazing control of phytoplankton biomass when salinities are < 5 psu, but grazing rates may also vary due to ambient salinities > 5 psu. In spite of these limitations, the sensitivity analyses conducted for these parameters showed that grazing by *X. securis* remained an important loss process for each simulation (Fig. 13). *X. securis* grazing removed between 8% and 26% of the nitrogen pool of DIN and chl *a* from the estuary during the sampling period and in all cases was similar to or greater than the amount of nitrogen removed by hydrodynamic processes (Table 5). The nitrogen left in the upper estuary at the end of the sampling period (i.e., nitrogen remaining as DIN and chl *a* and that consumed by mussels) is greater compared to the nitrogen lost as

TABLE 5. Nitrogen lost from the estuary as dissolved inorganic nitrogen (DIN) and chlorophyll *a* (chl *a*) given as a percentage of the nitrogen pool (i.e., initial nitrogen and DIN inputs from river inflow) due to advection, longitudinal dispersion, vertical dispersion, grazing by *Xenostrobus securis*, and other biological losses parameterized using a quadratic loss term for the model simulations of the sensitivity analysis. The maximum phytoplankton growth rate (μ_{max}), grazing by *X. securis* (α), and quadratic loss term (ϕ) were varied by factors of $\pm$ 2.

Model term	$\mu_{max} \div 2$	$\mu_{max} \times 2$	$\alpha \div 2$	$\alpha \times 2$	$\phi \div 2$	$\phi \times 2$
Advection	6	5	5	6	5	5
Longitudinal dispersion	21	9	14	13	15	13
Vertical dispersion	15	5	9	9	10	9
Mussel grazing	10	13	8	26	19	12
Other biological losses	18	63	56	41	41	56
Nitrogen remaining	30	5	8	5	10	5

DIN and chl *a* due to hydrodynamic processes and remains relatively unchanged (Table 5). Even when possible errors associated with estimating biological parameters are considered, it can be concluded that the demise of the phytoplankton bloom after day 10 was primarily due to biological, not hydrodynamic, processes.

The largest loss term for phytoplankton was the quadratic mortality term (Fig. 11). The magnitude of this term is adjusted to obtain a good fit with observations. Given independent knowledge of the magnitude of transport terms and *X. securis* grazing, this adjustment represents a use of the observed DIN and chl *a* to estimate the magnitude of unrepresented local biological loss processes. These may include endogenous respiration, nonpredatory mortality, settling, and grazing by zooplankton. The contribution of endogenous respiration and nonpredatory mortality to phytoplankton loss would be greater towards the end of the sampling period when growth becomes nitrogen limited and salinities increase. Settling may be important towards the end of the sampling period when river flow decreases, reducing mixing in the top boxes such that it cannot counter the settling loss of phytoplankton (Lucas et al. 1998). Zooplankton grazing may also become important towards the end of the sampling period if zooplankton communities are returned to the upper water layer by vertical mixing with bottom waters. The initial increase in river flow after the storm may dilute or even export resident zooplankton communities in the upper water layer. Depending on the strength of vertical mixing, zooplankton productivity, and survival in the fresher surface layer, zooplankton grazing may exert some top-down control on the bloom.

The box model only receives external sources of nitrogen from the river draining the upper catchment and the ocean. Underestimated model nitrogen towards the end of the sampling period may also be a result of internal inputs and processes not accounted for in the model, including nitrogen released from sediments under anoxic or hypoxic water conditions that is vertically dispersed into surface waters (Heggie et al. 1999) and the regeneration of nitrogen in the water column (Sanders et al. 1997). Mussels can contribute to the DIN pool in the water column via excretion of ammonia (Aldridge et al. 1995; Arnott and Vanni 1996; Babarro et al. 2000b). These biological, biochemical, and biogeochemical mechanisms regenerating nitrogen to the water column may explain the lower DIN concentrations in the model simulations.

This study assumes that the estuary is sectionally homogeneous, keeping the model to one dimension and disregarding any possible cross-sectional gradients in hydrodynamic properties. Grazing by *X. securis* is only possible at the lateral boundaries where mangrove pneumatophores occur. This could lead to a depletion of phytoplankton biomass at the edges of the estuary if horizontal dispersive processes are not sufficient to overcome any cross-sectional gradients that may result from the formation of a concentration boundary layer. If a boundary layer does develop by frictional retardation of flow around the mussels, then the grazing term by *X. securis* calculated here may be an overestimation. This has been shown to be an important mechanism in south San Francisco Bay reducing the effective clearance rate of subtidal filter-feeding bivalves when vertical mixing is slow (Koseff et al. 1993; Lucas et al. 1998). In south San Francisco Bay, vertical mixing has to overcome strong density gradients associated with vertical stratification. If a similar mechanism is occurring in the Wallamba River it is likely to be of lesser magnitude because horizontal mixing does not have to overcome density gradients, and so any cross-sectional gradients could be mixed by eddies and meanders at the surface. Also because the area of mangroves at the lateral boundaries is narrow (approximately 1 m), full horizontal mixing between the mangrove regions and the relatively narrow estuary channel is plausible. Further research should explicitly address this possibility.

Acknowledgments

The authors acknowledge the Australian Research Council (ARC) Strategic Partnership with Industry-Research and Training (SPIRT) program (No. C00107004). Industry partners are Great Lakes Council, Department of Environment and Conservation and the Department of Infrastructure, Planning and Natural Resources. M. B. was supported by ARC Discovery Project DP0209193. We thank our partner investigators G. Tuckerman, T. Pritchard, and G. Carter. Thanks to R. Piola, J. Everett, R. Moore, and K. Moore for assistance and support during field data collection and laboratory analyses. The Department of Public Works Manly Hydraulics Laboratory provided river height data, and the Department of Infrastructure, Planning and Natural Resources provided bathymetry data and a calibrated table to predict river flow from river height. We thank J. Giles for the size specific *Xenostrobus securis* distribution and abundance data for the Wallamba River. Thanks to J. Cloern and others for providing useful comments on earlier versions of the manuscript.

Literature Cited

Aldridge, D. W., B. S. Payne, and A. C. Miller. 1995. Oxygen consumption, nitrogenous excretion, and filtration rates of *Dreissena polymorpha* at acclimation temperatures between 20 and 32°C. *Canadian Journal of Fisheries and Aquatic Sciences* 52:1761–1767.

Allsop, D. and R. Kadluczka. 1999. Wallis Lake estuary tidal data collection March–June 1998. New South Wales Department of Public Works and Services and Manly Hydraulics Laboratory, MHL927, Manly Vale, Sydney, Australia.

Alpine, A. E. and J. E. Cloern. 1992. Trophic interactions and direct physical effects control phytoplankton biomass and production in an estuary. *Limnology and Oceanography* 37:946–955.

Arnott, D. L. and M. J. Vanni. 1996. Nitrogen and phosphorus recycling by the zebra mussel (*Dreissena polymorpha*) in the western basin of Lake Erie. *Canadian Journal of Fisheries and Aquatic Sciences* 53:646–659.

Babarro, J. M. F., M. J. Fernández-Reiriz, and U. Labarta. 2000a. Feeding behaviour of seed mussel *Mytilus galloprovincialis*: Environmental parameters and seed origin. *Journal of Shellfish Research* 19:195–201.

Babarro, J. M. F., M. J. Fernández-Reiriz, and U. Labarta. 2000b. Metabolism of the mussel *Mytilus galloprovincialis* from two origins in the Ría de Arousa (north-west Spain). *Journal of the Marine Biological Association of the United Kingdom* 80:865–872.

Basu, B. K. and F. R. Pick. 1996. Factors regulating phytoplankton and zooplankton biomass in temperate rivers. *Limnology and Oceanography* 41:1572–1577.

Bayne, B. L., R. J. Thompson, and J. Widdows. 1976. Physiology: I, p. 121–206. *In* B. L. Bayne (ed.), Marine Mussels: Their Ecology and Physiology. Cambridge University Press, Cambridge, Massachusetts.

Bridgeman, T. B., G. L. Fahnenstiel, G. A. Lang, and T. F. Nalepa. 1995. Zooplankton grazing during the zebra mussel (*Dreissena polymorpha*) colonization of Saginaw Bay, Lake Huron. *Journal of Great Lakes Research* 21:567–573.

Caraco, N. F., J. J. Cole, P. A. Raymond, D. L. Strayer, M. L. Pace, S. E. G. Findlay, and D. T. Fischer. 1997. Zebra mussel invasion in a large, turbid river: Phytoplankton response to increased grazing. *Ecology* 78:588–602.

Cloern, J. E. 1982. Does the benthos control phytoplankton biomass in south San Francisco Bay? *Marine Ecology Progress Series* 9:191–202.

Cloern, J. E. 2001. Our evolving conceptual model of the coastal eutrophication problem. *Marine Ecology Progress Series* 210:223–253.

Cloern, J. E., B. E. Cole, R. L. Wong, and A. E. Alpine. 1985. Temporal dynamics of estuarine phytoplankton: A case study of San Francisco Bay. *Hydrobiologia* 129:153–176.

Eyre, B. D. 2000. Regional evaluation of nutrient transformation and phytoplankton growth in nine river-dominated sub-tropical east Australian estuaries. *Marine Ecology Progress Series* 205:61–83.

Eyre, B. D. and D. Pont. 2003. Intra- and inter-annual variability in the different forms of diffuse nitrogen and phosphorous delivered to seven sub-tropical east Australian estuaries. *Estuarine Coastal and Shelf Science* 57:137–148.

Eyre, B. D. and C. Twigg. 1997. Nutrient behaviour during post-flood recovery of the Richmond River estuary northern NSW, Australia. *Estuarine Coastal and Shelf Science* 44:311–326.

Fasham, M., H. Ducklow, and S. McKelvie. 1990. A nitrogen-based model of plankton dynamics in the oceanic mixed layer. *Journal of Marine Research* 48:591–639.

Ferguson, A., B. D. Eyre, and J. Gay. 2004. Nutrient cycling in the sub-tropical Brunswick Estuary, Australia. *Estuaries* 27:1–17.

Figueiras, F. G., U. Labarta, and M. J. Fernández-Reiriz. 2002. Coastal upwelling, primary production and mussel growth in the Rías Baixas of Galicia. *Hydrobiologia* 484:121–131.

Fréchette, M. and E. Bourget. 1985. Energy flow between the pelagic and benthic zones: Factors controlling particulate organic matter available to an inter-tidal mussel bed. *Canadian Journal of Fisheries and Aquatic Sciences* 42:1158–1165.

Giles, J. 2002. The roles of salinity and predation on the size structure and distribution of the pygmy mussel *Xenostrobus securis*. Honours thesis, University of New South Wales Sydney, Australia.

Graham, J. M. 2000. Phytoplankton ecology, p. 547. *In* L. E. Graham and L. W. Wilcox (eds.), Algae. Prentice Hall, Upper Saddle River, New Jersey.

Hagy, J. D., L. P. Sanford, and W. R. Boynton. 2000. Estimation of net physical transport and hydraulic residence times for a coastal plain estuary using box models. *Estuaries* 23:328–340.

Jeffrey, S. W. and G. Humphrey. 1975. New spectrophotometric equations for determining chlorophylls a, b, c1, and c2 in higher plants, algae and natural phytoplankton. *Biochemie und Physiologie der Pfanzen* 167:191–194.

Hama, J. and N. Handa. 1994. Variability of the biomass, chemical composition and productivity of phytoplankton in Kinu-ura Bay, Japan during the rainy season. *Estuarine Coastal and Shelf Science* 39:497–509.

Heggie, D. T., G. W. Skyring, J. Orchardo, A. R. Longmore, G. J. Nicholson, and W. M. Berelson. 1999. Denitrification and denitrifying efficiencies in sediments of Port Phillip Bay: Direct determinations of biogenic N_2 and N-metabolite fluxes with implications for water quality. *Marine and Freshwater Research* 50:589–596.

Horgan, M. J. and E. L. Mills. 1997. Clearance rates and filtering activity of zebra mussel (*Dreissena polymorpha*): Implications for freshwater lakes. *Canadian Journal of Fisheries and Aquatic Sciences* 54:249–255.

Jassby, A. D., T. M. Powell, and C. R. Goldman. 1990. Interannual fluctuations in primary production: Direct physical effects and the trophic cascade at Castle Lake, California. *Limnology and Oceanography* 35:1021–1038.

Koseff, J. R., J. K. Holen, S. G. Monismith, and J. E. Cloern. 1993. Coupled effects of vertical mixing and benthic grazing on phytoplankton populations in shallow, turbid estuaries. *Journal of Marine Research* 51:843–868.

Kryger, J. and H. U. Riisgard. 1988. Filtration rate capacities in 6 species of European freshwater bivalves. *Oecologia* 77:34–38.

Lucas, L. V., J. E. Cloern, J. R. Koseff, S. G. Monismith, and J. K. Thompson. 1998. Does the Sverdrup critical depth model explain bloom dynamics in estuaries? *Journal of Marine Research* 56:375–415.

Lucas, L. V., J. R. Koseff, J. E. Cloern, S. G. Monismith, and J. K. Thompson. 1999a. Processes governing phytoplankton blooms

in estuaries. I: The local production-loss balance. *Marine Ecology Progress Series* 187:1–15.

LUCAS, L. V., J. R. KOSEFF, S. G. MONISMITH, J. E. CLOERN, AND J. K. THOMPSON. 1999b. Processes governing phytoplankton blooms in estuaries. II: The role of horizontal transport. *Marine Ecology Progress Series* 187:17–30.

MALLIN, M. A., H. W. PAERL, J. RUDEK, AND P. W. BATES. 1993. Regulation of estuarine primary productivity by watershed rainfall and river flow. *Marine Ecology Progress Series* 93:199–203.

OFFICER, C. B. 1980. Box models revisited, p. 65–114. *In* P. Hamilton and K. B. Macdonald (eds.), Estuarine and Wetland Processes, with Emphasis on Modeling, Volume 11. Plenum Press, New York.

REDFIELD, A. C., B. H. KETCHUM, AND F. A. RICHARDS. 1963. The influence of organisms on the composition of sea water, p. 26–79. *In* M. N. Hill (ed.), The Sea, Volume 2. Wiley Interscience, New York.

ROBSON, B. J. AND D. P. HAMILTON. 2003. Summer flow event induces a cyanobacterial bloom in a seasonal western Australian estuary. *Marine and Freshwater Research* 54:139–151.

RODITI, H. A., N. F. CARACO, J. J. COLE, AND D. L. STRAYER. 1996. Filtration of Hudson River water by the zebra mussel. *Estuaries* 19:824–832.

ROSON, G., X. A. ALVAREZ-SALGADO, AND F. F. PEREZ. 1997. A non-stationary box model to determine residual fluxes in a partially mixed estuary, based on both thermohaline properties: Application to the Ria de Arousa (Spain). *Estuarine Coastal and Shelf Science* 44:249–262.

SANDERS, R., C. KLEIN, AND T. JICKELLS. 1997. Biogeochemical nutrient cycling in the upper Great Ouse Estuary, Norfolk, U.K. *Estuarine Coastal and Shelf Science* 44:543–555.

SCHARLER, U. M. AND D. BAIRD. 2003. The influence of catchment management on salinity, nutrient stochiometry and phytoplankton biomass of Eastern Cape estuaries, South Africa. *Estuarine Coastal and Shelf Science* 56:735–748.

SMAAL, A. C. AND M. R. VAN STRALEN. 1990. Average annual growth and condition of mussels as a function of food source. *Hydrobiologia* 195:179–188.

SMITH, S. V. AND M. J. ATKINSON. 1983. Mass balance of carbon and phosphorus in Shark Bay, WA. *Limnology and Oceanography* 28:625–639.

SMITH, S. V. AND H. H. VEEH. 1989. Mass balance of biogeochemically active materials (C, N, P) in a hypersaline gulf. *Estuarine Coastal and Shelf Science* 29:195–215.

STEELE, J. H. AND C. W. CLARK. 1998. Relationship between individual- and population-based plankton models. *Journal of Plankton Research* 20:1403–1415.

WILSON, B. R. 1968. Survival and reproduction of the mussel *Xenostrobus securis* (Lamarck) (Mollusca: Bivalvia: Mytilidae) in a western Australian estuary. Part I. Salinity tolerance. *Journal of Natural History* 2:307–328.

WILSON, B. R. 1969. Survival and reproduction of the mussel *Xenostrobus securis* (Lamarck) (Mollusca: Bivalvia: Mytilidae) in a western Australian estuary. Pt. II: Reproduction, growth and longevity. *Journal of Natural History* 3:93–120.

SOURCES OF UNPUBLISHED MATERIALS

BUREAU OF METEOROLOGY. unpublished data. 700 Collins Street, Docklands, VIC 3008, Australia.

STANDARD METHODS FOR THE EXAMINATION OF WATER AND WASTEWATER. unpublished data. 1992. American Public Health Association, 1015 Fifteenth Street, NW, Washington, D.C. 20005.

DEPARTMENT OF INFRASTRUCTURE, PLANNING AND NATURAL RESOURCES. unpublished data. 23–33 Bridge Street, Sydney NSW 2000, Australia.

Received, February 15, 2005
Revised, July 25, 2005
Accepted, October 5, 2005